CrystEngComm

Accepted Manuscript

ROYAL SOCIETY OF CHEMISTRY

www.rsc.org/crystengcomm

Cite this: DOI: 10.1039/c0xx00000x

www.rsc.org/xxxxxx

ARTICLE TYPE

3D Hierarchical anatase TiO_2 superstructures constructed by "nanobricks" built nanosheets with exposed {001} facets: facile synthesis, formation mechanism and superior photocatalytic activity

Guoliang Li,[a] Jiyan Liu,[b] Jing Lan,[c] Gang Li,[b] Qiuwen Chen*[a] and Guibin Jiang[b]

Received (in XXX, XXX) Xth XXXXXXXXX 20XX, Accepted Xth XXXXXXXXX 20XX
DOI: 10.1039/b000000x

Exploring anatase TiO_2 with superior photocatalytic activity is of great value and challenging. 3D hierarchical anatase TiO_2 with a high percentage of exposed {001}S facets has been successfully synthesized through a simple one-pot solvothermal strategy in presence of ammonium fluoride and ethylene glycol solution. It was found both NH_4F and ethylene glycol played an essential role in directing 3D hierarchical structure with exposed {001} facets. Characterization by SEM, TEM, XRD, and TG endorsed a plausible proposed formation mechanism of "nucleation-aggregation-recrystallization". The product was proved exhibiting superior photocatalytic activity under the synergistic effect of improved light-harvesting ability and higher reactivity of exposed {001} facets.

1 Introduction

Titanium dioxide (TiO_2), as one of the most promising semiconductors, has been extensively and deeply studied due to its high catalytic activity, long-term stability and great versatility in various fields, such as photocatalysis, photovoltaic cells, sensors, Li-ion battery materials and so on.[1-7] It has been found that application efficiency of TiO_2 depends strongly on the shape, size and exposed facets.[8-10] Therefore, controllable synthesis of TiO_2 of different morphologies and specific exposed facets has drawn more and more attention to make better use of the prepared products.[11-14] Recently, both theoretical and experimental studies of anatase TiO_2 show that the metastable {001} facets are more reactive compared to other facets.[15,16] Unfortunately, most common and easily synthesized anatase TiO_2 crystals are dominated by the thermodynamically stable {101} facets, which make up more than 94% of the total surface area.[17] High reactivity makes the synthesis of {001} facets dominated anatase crystals a significant challenge because these high energy facets shrink and disappear quickly during crystal growth to minimize the Gibbs energy. Only recently, a pioneering work by Yang et al. introduced a method to synthesize TiO_2 single microcrystals with 47% exposed {001} facets by using TiF_4 as the raw material and hydrofluoric acid as the morphology controlling reagent.[15] Since then, many studies have been conducted to synthesize anatase TiO_2 of different structures (e.g. nanoparticles, nanorods, micro-/nano sheets, and nanotubes) with exposed {001} facets.[18-23] However, most of these synthesized anatase TiO_2 are crystals of two-dimensionality with poor light harvesting ability, only a few attempts have been made toward obtaining three-dimensional microsize superstructures constructed by nanoscale primary subunits. In addition, to our knowledge, specific surfactants or other structure-directing reagents like toxic etching HF are usually applied to fulfil the synthetic process.[12,15,24] Hence, it is still a great challenge to explore more facile and greener method to synthesize anatase TiO_2 with hierarchical structures and high percentage of exposed {001} facets. In this work, we aimed at presenting a convenient procedure for synthesis of 3D hierarchical titania superstructures (3DHTS) constructed by microscale nanosheets, which were further orderly built by nanoscale subunits with exposed {001} facets. What is more, no surfactant or other structure-directing reagents were used. Photocatalytic experiment was also performed to demonstrate the superior photo-degradation towards organic-dye Rhodamine B.

2 Experimental

2.1 Materials synthesis

In a typical experimental procedure, 20 mmol NH_4F was added into 5 mL deionized water and was magnetically stirred until completely dissolved, followed by addition of 50 mL ethylene glycol (EG). After string for 15 min, 5 mmol $TiOSO_4$ (Sigma-Aldrich Corp (No.495379)) was added into the solution and magnetically stirred for 10 min. Then, the mixture solution was transferred into a 100 mL Teflon pot and sealed tightly in a stainless steel autoclave and heated to 200 ^oC with an increase rate of 3 ^oC min^{-1}. After 12 hrs' solvothermal treatment at 200 ^oC, the autoclave was removed from the oven and cooled in the air to room temperature. Then, the products were washed with absolute ethanol and distilled water 3 times, respectively. The white precipitates were collected and vacuum dried at 80 ^oC overnight and kept in a desiccator for further use. A portion of the white powder was then calcined in a Muffle furnace at 450 ^oC for 1.5 h with a ramping rate of 5 ^oC min^{-1}. The samples were then cooled to room temperature and kept in a desiccator for characterization

and application.

2.2 Materials characterization

Morphological observations were performed on a field-emission electron microscope (SU8000, Hitachi, Japan). Transmission electron microscopy (TEM) and high resolution transmission electron microscopy (HRTEM) analysis were carried out on a JEM-2100 (JEOL, Japan) using a 200 kV accelerating voltage. The X-ray diffraction (XRD) pattern was recorded with a PANalytical X'Pert Pro X-ray diffractometer (PANalytical, Netherland) equipped with Cu-Ka radiation (40kV, 200 mA) to characterize the crystalline phase, phase composition, and crystallite size of the TiO_2 powder. The TG/DSC was examined on a Netzsch STA449 instrument from room temperature to 800 ^oC with a heating rate of 10 ^oC min^{-1}. The X-ray photochemical spectra was performed on a Thermo SCIENTIFIC ESCALAB 250 equipped with Al-Ka alpha radiation. Nitrogen adsorption-desorption isotherms were measured with a Micromeritics ASAP2000 V3.01 analyser. The Brunauer-Emmett-Teller (BET) specific surface area was measured by nitrogen adsorption in a Micromeritics ASAP 2020 nitrogen adsorption apparatus. All samples were degassed at 120 ^oC prior to nitrogen adsorption measurements. The specific surface area was calculated using the BET equation. The pore size distribution was obtained using the Barret-Joyner-Halenda (BJH) equation. UV-vis diffuse reflection spectra (UV-vis DSR) was performed on a Hitachi U4100 spectrometer.

2.3 Photocatalytic activity

Photocatalytic activity of the 3DHTS were examined by degradation of azo-dye Rhodamine B (Rh.B) at room temperature in a fume cupboard which was pre-wrapped with Al foil simulating a "dark room" to avoid exposure of the Rh.B solutions to visible light. An 8W mercury lamp with characteristic wavelength of 365 nm was placed beside the custom-made quartzose reactor as light source. 0.05 g 3DHTSs were added into 50 mL Rh.B solution (10 mg L^{-1}) in the reactor and magnetically stirred at a speed of 800 rpm for 1 h to ensure the adsorption equilibrium and eliminate the diffusion effects. Then, the mixture solution was irradiated. Samples were taken at an interval of 15 min, filtered through a 0.2 um cellulose acetate membrane and detected by UV-Vis spectroscope (Hitachi U4100, Japan).

3 Results and discussion

Fig. 1 shows the scanning electron microscopy (SEM), transmission electron microscopy (TEM) and high-resolution transmission electron microscopy (HRTEM) images of the 3DHTS. SEM image (Fig. S1) indicates the products are of uniform hierarchical structure with an average diameter of 8 μm. Fig. 1a reveals that the as-prepared 3DHTS are composed of randomly arranged TiO_2 nanosheets which are constructed by monolayer of nanoscale rice-grain like TiO_2 "nanobricks" of about 50 nm in length and 30 nm in width (Fig. 1b). A three dimensional superstructure was constructed by these interconnected nanosheets forming pores of different sizes, which supplies transport paths for small molecules. The abovementioned microstructures of the 3DHTS were also characterized by TEM. Fig. 1c and Fig. 1d further confirmed the entire structure of the architecture was built from self-organized TiO_2 nanosheets and the subunits of nanoscale particles. Representative high resolution TEM images of a single nanosheet are shown in Fig. 1e and Fig. 1f. Fig. 1e shows that the lattice spacing parallel to the top and bottom facets was 0.19 nm, corresponding to the (001) planes, which indicates the top and bottom facets of the nanosheets are assigned to (001) planes of anatase TiO_2. Furthermore, the HRTEM image of the vertical nanosheets shows another set of lattice fringes spacing of 0.35 nm, corresponding to the (101) planes of anatase TiO_2. Based on the above structure information, the percentage of the exposed (001) facets of the products can be estimated by a reported method to be over 90%.[25]

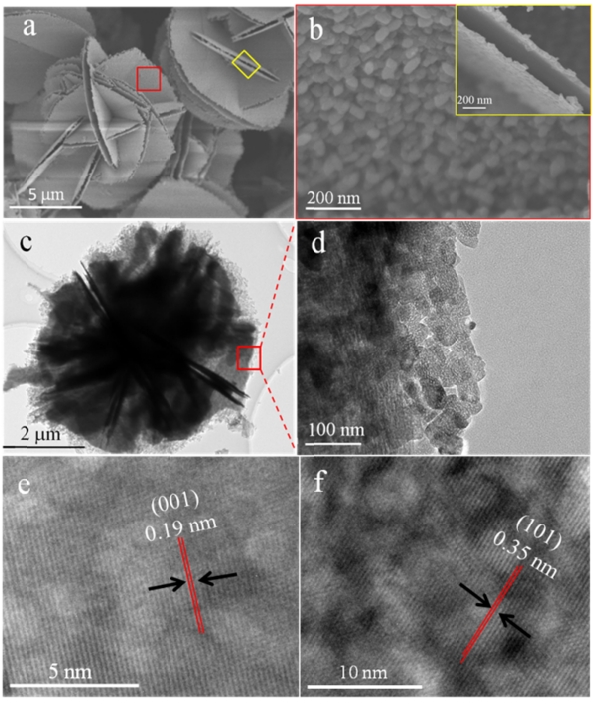

Fig. 1 SEM (a, b), TEM (c, d) and high-resolution TEM (e, f) images of the 3DHTS.

As illustrated in Fig. 2, the crystallographic structure of the product before and after calcination were characterized by powder X-ray diffraction (XRD). For XRD patterns of the prepared sample before calcination, diffraction peaks around 2θ = 25.5, 38, 47.8, 54, and 55.4^o can be ascribed to anatase TiO_2 (JCPDS no. 21-1272). All the other peaks are consistent with the JCPDS file no. 52-1674, which represents orthorhombic NH_4TiOF_3 (space group: Pbmn, a = 0.7552, b = 0.7584, c = 6.3038 nm). Therefore, the prepared precursor is a mixture of NH_4TiOF_3 and TiO_2 crystals. While the sample crystals after calcination can be assigned to the anatase TiO_2 phase (space group I41/amd) with no peaks of other compounds can be found, which indicates NH_4TiOF_3 was completely converted into TiO_2 after calcination treatment. Notable broadening of the (004) diffraction peak can be easily identified in the XRD pattern, indicating a small size along the [001] crystallographic direction. What is more, broadening of the diffraction peak along the [100] crystallographic direction does not occur. Compared with that of the bulk anatase TiO_2 (JCPDS no. 21-1272), the relative diffraction intensity of (200) is much higher. These results indicate that the as-prepared anatase TiO_2 has anisotropic sheet-

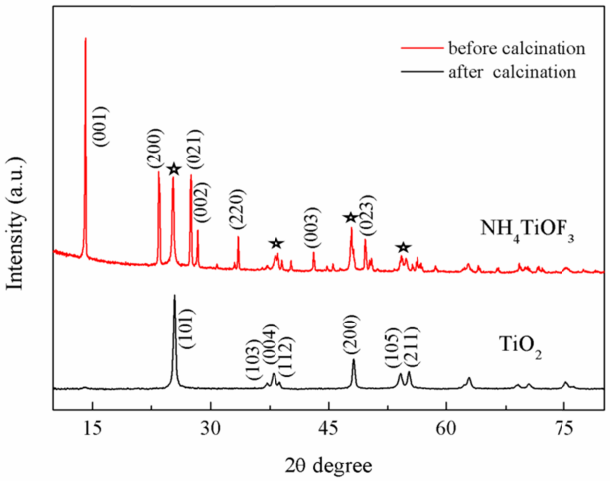

Fig. 2 XRD patterns of the 3DHTS before and after calcination.

like building units.[24] The crystallite size calculated using Scherrer formula was 30.2 nm which is in good accordance with the SEM and TEM results. TG/DSC was performed to better understand the thermal conversion process. Fig. S2 shows the conversion process undergoes 4 steps. In the first step (25-228 °C), impurities such as water, ethanol and other volatile components were removed. The second step falls between 228 to 327 °C, during which NH_4TiOF_3 was pyrolyzed to $HTiOF_3$. Then, it came to the third stage (327-391 °C), $HTiOF_3$ was converted to $TiOF_2$. At last, $TiOF_2$ was fully pyrolyzed to TiO_2.

The surface composition and chemical status of the product was characterized by X-ray photoelectronic spectrum (XPS). As illustrated in Fig. 3, four characteristic peaks of Ti, O, F and C were observed. The binding energy of Ti 2P3/2 and Ti 2P1/2 is 458.3 and 464.1 eV, indicating the oxidation state of the Ti element is the same as that of bulk TiO_2. The high resolution XPS spectrum of the F1s region is shown in Fig. 3c with a binding energy of 683.7 eV, which is a typical value for fluorinated TiO_2 systems, such as ≡Ti-F species on the TiO_2 crystal surface.[26] However, the binding energy of F1s for atomic incorporation of F

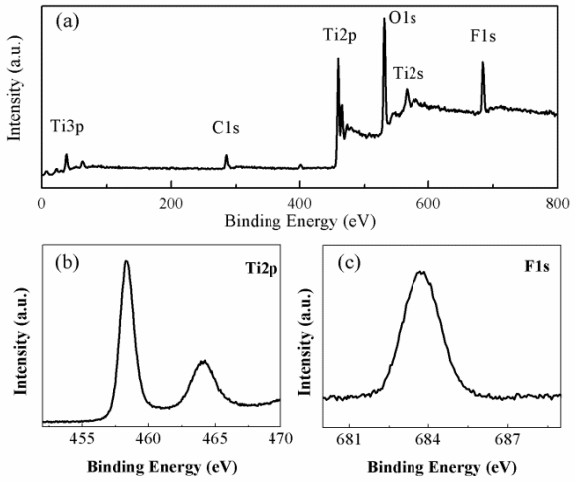

Fig. 3 XPS survey spectra (a) and the high-resolution XPS spectra of Ti2p (b) and F1s (c) of the 3DHTS.

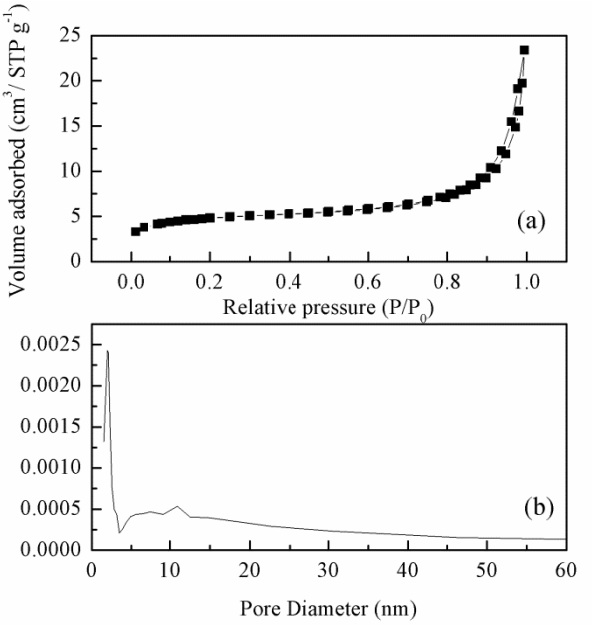

Fig. 4 N_2 adsorption-desorption isotherms (a) and the pore size distribution curve (b) of the 3DHTS.

atoms or their substitution for O atoms is 688.5 eV.[19] Therefore, it can be concluded that F element is present as surface atoms. The carbon peak is attributed to the residual carbon of the product and the adventitious hydrocarbon from the XPS instrument itself.

N_2 adsorption-desorption analysis was also performed to determine the porous structure and texture of the 3DHTS. Fig. 4 displays N_2 adsorption-desorption isotherms and the corresponding BJH pore size distribution curve for the product. The isotherms exhibit the typical type □ curve with a H3 hysteresis loop according to the IUPAC classification, which is usually ascribed to slit-like mesopores (2-50 nm) by sheet-like particles.[27] The Barrett-Joyner-Halenda (BJH) pore distribution obtained from the isotherms indicates the product contains two types of pores. One type of pore may be ascribed to a larger portion of mesopores (~2.1 nm) derived from assembly of the small TiO_2 nanoparticles. The other type of pore (~10.8 nm) may be attributed not only to the randomly assembled nanosheets composed of nanoparticle buildings, but also to the voids resulted from inter-aggregation of samples.

The formation mechanism of the as-prepared nanosheets based 3D hierarchical structure was investigated by time-dependent experiments. It was generally popular to elucidate the formation of such 3D hierarchical structure with a two-stage growth mechanism, which involves the initial formation of 2D nanostructures and the subsequent self-assembly process.[24,28] However, our experimental results show a different formation route. At the initial stage (2 h) of the reaction, a large number of small nanoparticles of several nanometers in diameter (Fig. 5a) were firstly nucleated at a very fast rate due to fast hydrolyzation of the $TiOSO_4$. When the reaction time prolonged to 4 h, these nanoparticles induced a high collision frequency to reduce the system energy, leading to a random agglomeration of the particles forming flakes interconnected cross-linked structures (Fig. 5b). Further extended the reaction time to 8 h, with decrease of the particle number density, the particles started to aggregate in a

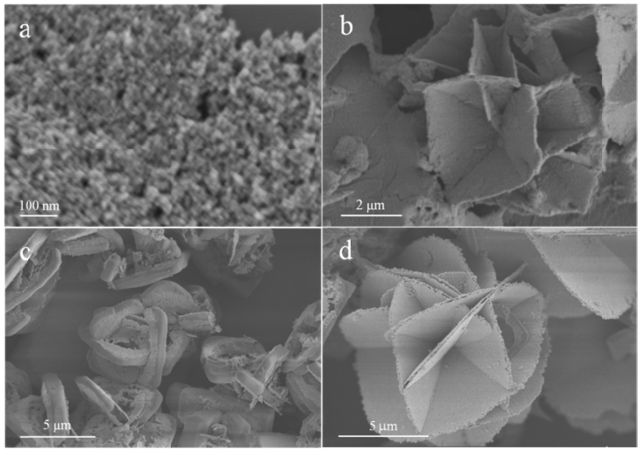

Fig. 5 SEM images of the samples obtained at different reaction time: (a) 2, (b) 4, (c) 8, and (d) 12 h.

more ordered fashion eliminating the solid-solution interface to further minimize the system energy. This behaviour corresponds to the formation of cross-linked architecture at the expense of extra nanoparticles (Fig. 5c). With the reaction time continuing to 12 h, smaller particles of higher energy near the surface of the plate can dissolve easily and release outwards. When a significant quantity of "ordered" attachment has taken place, the released ions may be numerous enough to increase the supersaturation and induce a second nucleation as modelled by Nomura et al.[29] Then thicker flakes undergone a "re-crystallization" process, during which the surface of the thick flakes became more crystallized due to full involvement into the solvothermal reaction. Meanwhile, the poor-crystallized inner part of the thick flakes tended to gradually dissolve and simultaneously take part in the surface-recrystallizing process, and therefore forming larger nanosheets based 3D hierarchical superstructures (Fig. 5d). As to the formation of {001} facets, it can be attributed to the capping effect of F ions and EG. During the solvothermal reaction, NH_4TiOF_3 nuclei were formed instead of TiO_2 and thus led to the formation of NH_4TiOF_3 crystals (Eqs. (1)-(4)).

$$2NH_4F + H_2SO_4 \rightleftharpoons 2HF + (NH_4)_2SO_4 \quad (1)$$

$$TiOSO_4 + 6HF \rightleftharpoons [TiF_6]^{2-} + 4H^+ + SO_4^{2-} + H_2O \quad (2)$$

$$[TiF_6]^{2-} + 3H_2O \rightleftharpoons [Ti(OH)_3F_3]^{2-} + 3HF \quad (3)$$

$$[Ti(OH)_3F_3]^{2-} + H^+ + NH_4^+ \rightleftharpoons NH_4TiOF_3 \downarrow + 2H_2O \quad (4)$$

In absence of EG or even increased the dose of water in the reaction system, the concentration of F^- is too low to restrain the growth of NH_4TiOF_3 nuclei along the [001] direction forming anomalous particles (Fig. S3). In acidic environment, EG has a tendency to heterolytically dissociate into $^-OCH_2CH_2O^-$, which accompanying with F^- preferentially bind to unsaturated Ti^{4+} cations on {001} facets and thus restraining growth along the [001] direction. Instead, faster growth along [101] and [100] directions will lead to formation of nanosheets with exposed {001} facets.

Photocatalytic activity of the prepared 3DHTS was evaluated by the photo-degradation of a probe organic pollutant, azo-dye Rhodamine B (Rh.B), under UV light irradiation. The photocatalytic activity of a well-known highly efficient commercial titania photocatalyst, Degussa P25, was also measured under the same condition for comparison. Fig. 6

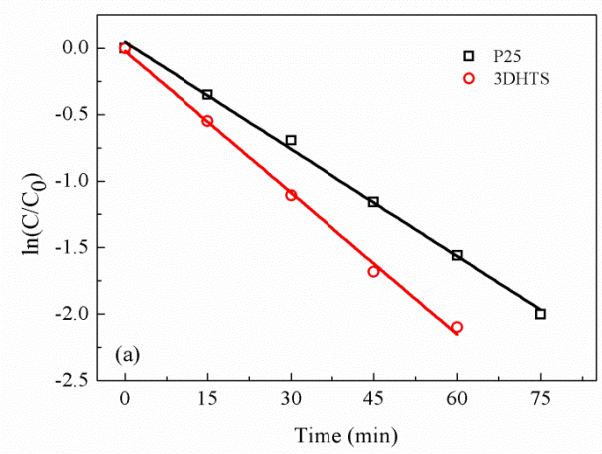

Fig. 6 Photocatalytic degradation of Rh.B in presence of the 3DHTS and Degussa P25.

exhibits the reaction kinetics of the Rh.B degradation. A pseudo-first-order kinetics equation, $\ln(C/C_0)=kt$ (C and C_0 represent the concentration of Rh.B at the irradiation time t and 0 mintes, k and t refer to the reaction rate constant and the reaction time, respectively), was applied to compare the reaction rates. As illustrated in Fig. 6, the plots fit well with the applied equation showing a linear pattern. The photo-degradation of Rh.B in presence of 3DHTS shows a much higher degradation rate (0.0351 min^{-1}) than the probe P25 (0.0268 min^{-1}) even under the circumstance that the 3DHTS obtain lower specific surface area 22.65 $m^2\ g^{-1}$) than that of the Degussa P25 (48 $m^2\ g^{-1}$). As schematically illustrated in Fig. S4, the crosslinked nanosheets provide for multiple reflections of UV light, which can maximize light harvesting and thus increase the quantities of photogenerated electrons and the holes functioning in the photocatalytic reactions.[27,28] This result was also confirmed by the UV-vis diffuse reflectance spectra (UV-Vis DRS, Fig. S5) of the 3DHTS, which clearly indicates the 3DHTS possess a stronger absorbance in UV region than the nanoscale P25 particles. Based on the above results, the superior photocatalytic activity of the 3DHTS could be elucidated as a synergistic effects of the following 3 aspects: 1) the existence of 2D nanosheets with exposed {001} facets that has been theoretically and experimentally proved to be more reactive than the thermodynatically more stable {101} facets could enhance the adsorption of pollutant molecules and thus lead to the enhancement of photocatalytic activity;[15,30] 2) the unique 3D hierarchical structure composed of crosslinked 2D nanosheets provide for multiple reflections of UV light, which can maximize light harvesting and thus increase the quantities of photogenerated electrons and the holes functioning in the potocatalytic reactions;[31,32] 3) the nanosheets based porous intermeshed networks supply diffusion paths for pollutants and the degradation outcomes to travel through the material and therefore not only accelerate the mass exchange rate but also promote accessibility of pollutant to the active surface sites.

4 Conclusions

A simple one-pot approach for synthesis of 3D hierarchical TiO_2 superstructures with exposed {001} facets has been developed,

which features convenient control and absence of surfactant or other structure-directing reagents. F ions accompanied with heterolytically dissociated EG retarded the growth of TiO_2 along [001] direction. As-synthesized 3DHTS was constructed by 2D microscale nanosheets which were further composed of 1D nanoscale rice-grain like "bricks" and possessed high percentage of exposed high energy {001} facets. This unique structure not only results in porous texture supplying diffusion paths for pollutants and the degradation outcomes to travel through the material, but also improves light harvesting ability through multi-reflection. Thus, the synergistic effect of these features endows the prepared 3DHTS with superior photocatalytic activity.

Acknowledgements

This work was financially supported by the National Nature Science Foundation of China (No. 21207148) and the National Basic Research Program of China (No. 2011CB936001).

Notes and references

[a] *State Key Laboratory of Environmental Aquatic Chemistry, Research Center for Eco-Environmental Sciences, Chinese Academy of Sciences, P.O. Box 2871, Beijing 100085, P. R. China; E-mail: qchen@rcees.ac.cn; Tel:8610-62849311.*

[b] *State Key Laboratory of Environmental Chemistry and Ecotoxicology, Research Center for Eco-Environment Sciences, Chinese Academy of Sciences, Beijing 100085, P. R. China.*

c College of Chemistry and Pharmaceutical Sciences, Qingdao Agricultural University, Qingdao 266109, P. R. China.

† Electronic Supplementary Information (ESI) available: supplementary images of SEM, TG-DSC, schematic illustration of light reflection and UV-Vis DRS curves. See DOI: 10.1039/b000000x/

1. J. B. Joo, M. Dahl, N. Li, F. Zaera and Y. Yin, *Energy Environ. Sci.*, 2013, **6**, 2082-2092.
2. G. Li, H. Zhang, J. Lan, J. Li, Q. Chen, J. Liu and G. Jiang, *Dalton Trans.*, 2013, **42**, 8541-8544.
3. Z. Y. Weng, H. Guo, X. M. Liu, S. L. Wu, K. W. K. Yeung and P. K. Chu, *RSC Adv.*, 2013, **3**, 24758-24775.
4. A. J. Frank, N. Kopidakis and J. van de Lagemaat, *Coord. Chem. Rev*., 2004, **248**, 1165-1179.
5. X. Chen and S. S. Mao, *Chem. Rev.*, 2007, **107**, 2891-2959.
6. G. Li, J. Liu and G. Jiang, *Chem. Commun.*, 2011, **47**, 7443-7445.
7. M. Epifani, T. Andreu, R. Zamani, J. Arbiol, E. Comini, P. Siciliano, G. Faglia and J. R. Morante, *Crystengcomm*, 2012, **14**, 3882-3887.
8. G. Cernuto, N. Masciocchi, A. Cervellino, G. M. Colonna and A. Guagliardi, *J. Am. Chem. Soc.*, 2011, **133**, 3114-3119.
9. N. Wu, J. Wang, D. N. Tafen, H. Wang, J.-G. Zheng, J. P. Lewis, X. Liu, S. S. Leonard and A. Manivannan, *J. Am. Chem. Soc.*, 2010, **132**, 6679-6685.
10. J. M. Du, J. S. Zhang and D. J. Kang, *Crystengcomm*, 2011, **13**, 4270-4275.
11. M. Liu, L. Y. Piao, L. Zhao, S. T. Ju, Z. J. Yan, T. He, C. L. Zhou and W. J. Wang, *Chem. Commun*., 2010, **46**, 1664-1666.
12. M. Liu, L. Piao, W. Lu, S. Ju, L. Zhao, C. Zhou, H. Li and W. Wang, *Nanoscale*, 2010, **2**, 1115-1117.
13. X. Yao, X. Liu, T. Liu, K. Wang and L. Lu, *Crystengcomm*, 2013, **15**, 10246-10254.
14. G. H. Tian, Y. J. Chen, W. Zhou, K. Pan, C. G. Tian, X. R. Huang and H. G. Fu, *Crystengcomm*, 2011, **13**, 2994-3000.
15. H. G. Yang, C. H. Sun, S. Z. Qiao, J. Zou, G. Liu, S. C. Smith, H. M. Cheng and G. Q. Lu, *Nature*, 2008, **453**, 638-641.
16. Q. J. Xiang, J. G. Yu and M. Jaroniec, *Chem. Commun*., 2011, **47**, 4532-4534.
17. M. Lazzeri, A. Vittadini and A. Selloni, *Phys. Rev. B*, 2001, **63**, 155409.
18. W. Yang, J. Li, Y. Wang, F. Zhu, W. Shi, F. Wan and D. Xu, *Chem. Commun.*, 2011, **47**, 1809-1811.
19. Z. Zheng, B. Huang, J. Lu, X. Qin, X. Zhang and Y. Dai, *Chem. – Eur. J.*, 2011, **17**, 15032-15038.
20. W. J. Ong, L. L. Tan, S. P. Chai, S. T. Yong and A. R. Mohamed, *Nanoscale*, 2014, **6**, 1946-2008.
21. C. Hu, X. Zhang, W. T. Li, Y. Yan, G. C. Xi, H. F. Yang, J. F. Li and H. Bai, *J. Mater. Chem. A*, 2014, **2**, 2040-2043.
22. X. Wang, H. He, Y. Chen, J. Zhao and X. Zhang, *Appl. Surf. Sci.*, 2012, 258, 5863-5868.
23. L. Zhou, J. Chen, C. Ji, L. Zhou and P. O'Brien, Crystengcomm, 2013, **15**, 5012-5015.
24. W. Q. Fang, J. Z. Zhou, J. Liu, Z. G. Chen, C. Yang, C. H. Sun, G. R. Qian, J. Zou, S. Z. Qiao and H. G. Yang, *Chem. –Eur. J.*, 2011, **17**, 1423-1427.
25. B. Liu and E. S. Aydil, *Chem. Commun*., 2011, **47**, 9507-9509.
26. J. C. Yu, J. G. Yu, W. K. Ho, Z. T. Jiang and L. Z. Zhang, *Chem Mater*, 2002, **14**, 3808-3816.
27. M. Kruk and M. Jaroniec, *Chem Mater*, 2001, **13**, 3169-3183.
28. S.-W. Cao and Y.-J. Zhu, *J. Phys. Chem. C*, 2008, **112**, 12149-12156.
29. T. Nomura, Y. Kousaka, M. Alonso, M. Fukunaga and T. Satoh, *J. Colloid Interface Sci.*, 2000, **221**, 195-199.
30. S. Liu, J. Yu and M. Jaroniec, *J. Am. Chem. Soc.*, 2010, **132**, 11914-11916.
31. P. Jiang, J. J. Zhou, H. F. Fang, C. Y. Wang, Z. L. Wang and S. S. Xie, Adv. *Funct. Mater.*, 2007, **17**, 1303-1310.
32. Q. Xiang and J. Yu, *Chin. J. Catal.*, 2011, **32**, 525-531.